Path-Following Algorithms and Experiments for an Unmanned Surface Vehicle

Marco Bibuli, Gabriele Bruzzone, and Massimo Caccia
Istituto di Studi sui Sistemi Intelligenti per l'Automazione
Consiglio Nazionale delle Ricerche
Via De Marini 6
16149 Genova, Italy
e-mail: marco@ge.issia.cnr.it, gabry@ge.issia.cnr.it, max@ge.issia.cnr.it

Lionel Lapierre
Laboratoire d'Informatique, de Robotique et de Microlectronique de Montpellier
Centre National de la Recherche Scientifique
161 rue Ada
34392 Montpellier Cedex 5, France
e-mail: lapierre@lirmm.fr

Received 8 January 2009; accepted 4 May 2009

This paper addresses the problem of path following in two-dimensional space for underactuated unmanned surface vehicles (USVs), defining a set of guidance laws at the kinematic level. The proposed nonlinear Lyapunov-based control law yields convergence of the path-following error coordinates to zero. Furthermore, the introduction of a virtual controlled degree of freedom for the target to be followed on the path removes singularity behaviors present in other guidance algorithms proposed in the literature. Some heuristic approaches are then proposed to face the problem of speed of advance adaptation based on path curvature measurement and steering action prediction. Finally a set of experimental results of all the proposed guidance laws, carried out with the Charlie USV, demonstrates the feasibility of the proposed approach and the performance improvements, in terms of precision in following the reference path and transient reduction, obtained by introducing speed adaptation heuristics.

1. INTRODUCTION

In the past 15 years a large number of unmanned surface vehicles (USVs) have been developed for a large set of applications such as environmental monitoring and sampling, coastal protection, bathymetric surveys, and support for autonomous underwater vehicle (AUV) operations.

Some examples are given by the family of USVs at the MIT AUV Lab (Benjamin & Curcio, 2004; Manley, Marsh, Cornforth, & Wiseman, 2000); the flotilla of autonomous marine vehicles, such as

Delfim and Caravela, at the Lisbon IST–ISR Dynamical System and Ocean Robotics Laboratory (Alves et al., 1999; Pascoal et al., 2000); the Charlie USV originally developed by the Consiglio Nazionale delle Ricerche–Istituto di Studi sui Sistemi Intelligenti per l'Automazione (CNR–ISSIA) Genova for sea surface microlayer sampling and then applied to restricted water operations (Caccia et al., 2007); the ROAZ autonomous surface vehicles developed by the Instituto Superior de Engenharia do Porto, also devoted to search and rescue support (Martins, Almeida, Silva, & Pereira, 2006); and the catamaran Springer developed by Plymouth University to monitor and track water pollution (Xu, Chudley, & Sutton, 2006).

On the military side, the project SWIMS, i.e., shallow water influence mine sweeping system, by QinetiQ, Ltd., successfully demonstrated a conversion kit able to convert standard RIBs (rigid inflatable boats) in remotely controlled ones during the second Gulf War (Cornfield & Young, 2006). After that, research mainly focuses on the development and integration of sensors for over-the-water obstacle detection and avoidance. Examples are given by the test bed developed at SSC San Diego (Ebken, Bruch, & Lum, 2005), based on the Bombardier SeaDoo Challenger 2000, and the Israeli Protector USV,[1] equipped with radar and advanced electro-optical devices.

For major details about USV technology, the reader can refer to Caccia (2006) and Manley (2008). In this context, the existing prototype USVs, typically not equipped with side thrusters and thus underactuated, are required to perform tasks that need increasing maneuvering accuracy, moving, for instance, from the goal of executing an integral sampling in a relatively large area to the aim of reconstructing a very precise bathymetry of a littoral zone.

Pioneer applications, such as sea surface microlayer sampling carried out by CNR–ISSIA Charlie USV (Caccia et al., 2005) and cooperative autonomy trials performed with the SCOUT autonomous surface craft (ASC) (Curcio, Leonard, & Patrikalakis, 2005), demonstrated that basic autopilots, consisting of a simple proportional (integral) derivative [P(I)D] heading controller, are sufficient for guaranteeing satisfactory performance in controlling the horizontal motion of a USV. Still more advanced control techniques have been proposed in order to increase system robustness. A dual-nested-loop H_2 controller, in which the inner yaw rate loop guarantees stability, robustness, and disturbance rejection and the outer-position loop improves follow-up performance, has been satisfactorily applied to the course control of the MESSIN USV, an autonomous catamaran developed by the University of Rostock (Majohr & Buch, 2006). A more general approach, based on gain-scheduling controllers, interpolating the parameters of linear controllers designed at different forward speeds, has been proposed in Pascoal, Silvestre, and Oliveira (2006). In particular, the H_∞ performance criterion used for designing the linear controllers allows a unified treatment of control and motion estimation, performed through complementary filter techniques, in a frequency domain–based approach (Fryxell, Oliveira, Pascoal, Silvestre, & Kaminer, 1996).

As far as ship autopilots are concerned, research is, for obvious logistical reasons, typically carried out using simulation studies rather than actual vehicles. As thoroughly discussed in Roberts (2008), in spite of the efforts and enthusiasm of researchers in trying to persuade industry to adopt more sophisticated designs, proportional–integral–differential (PID) controllers remain the industrial standard for ship automatic control systems. Some advances are reported in the field-integrated fin rudder roll stabilization, when two control surfaces (rudder and stabilizing fins) are combined to simultaneously control roll and yaw motions. For instance, Roberts, Sharif, Sutton, and Agarwal (1997) present one of the first reported implementations of H_∞ controllers. Multiobjective optimization of PID and H_∞ controllers, as well as model predictive control, represents an advanced field of research, together with the development of adaptive and switched control systems for making the controller effective for all ship speeds, sea states, and wave encounter angles. More recently, leader companies offer advanced commercial solutions implementing adaptive heading and track control providing optimal steering behavior under all weather and load conditions.

On the other hand, the issue of guidance in the path scenario was recently overviewed in Breivik and Fossen (2008). Guidance is responsible for prescribing commands needed to achieve the motion control objectives in the physical environment in which a vehicle moves. To integrate the guidance system with classical autopilots, in the original formulation of tracking controllers, commands consisted of heading

[1]Protector—Unmanned Naval Patrol Vehicle. http://www.israeli-weapons.com/weapons/naval/protector/Protector.html.

set points, while, with the introduction of hierarchical control architectures decoupling kinematics and dynamics, guidance laws generate a reference yaw rate in addition to the desired surge speed. Thus, in this novel formulation the guidance module is called the kinematic controller.

In the literature, motion control scenarios of USVs were usually classified into three main categories (point stabilization, trajectory tracking, and path following):

- Point stabilization: The goal is to stabilize the vehicle, zeroing the position and orientation error with respect to a given target point, with a desired orientation. The goal cannot be achieved with smooth or continuous state-feedback control laws when the vehicle has nonholonomic constraints; in this case, approaches such as smooth time-varying control laws and discontinuous and hybrid feedback laws have been proposed.
- Trajectory tracking: The vehicle is required to track a time-parameterized reference. For a fully actuated system, the problem can be solved with advanced nonlinear control laws; in the case of underactuated vehicles, that is, the vehicle has fewer degrees of freedom than state variables to be tracked, the problem is still a very active topic of research.
- Path following: The vehicle is required to converge to and follow a path, without any temporal specification. The assumption made in this case is that the vehicle's forward speed tracks a desired speed profile, while the controller acts on the vehicle orientation to drive it to the path. This typically allows a smoother convergence to the desired path with respect to the trajectory tracking controllers, less likely pushing to saturation the control signals (Encarnaçao & Pascoal, 2001).

Because the requirement of following desired paths with great accuracy with a speed profile specified by the end user is sufficient for many applications, the problem of path following, i.e., steering a vehicle to converge to and follow a predefined path in the plane, is addressed in this paper.

The path-following problem, originally addressed in the literature in the case of wheeled robots, consists of defining, computing, and reducing to zero the distance between the vehicle and the path as well as the angle between the vector representing the vessel speed and the tangent to the desired path. In the case of unmanned marine vehicles, a solution based on gain-scheduling control theory and the linearization of a generalized error vector about trimming paths was proposed in Pascoal et al. (2006) and implemented and run on the Delfim Autonomous Surface Craft. After that, research focused on the development of nonlinear control design methods able to guarantee global, not only local, stability as in the above-mentioned approach.

In particular, research in this direction has been guided by the key idea of controlling the rate of progression of a "virtual target," also named the *rabbit*, that has to be tracked, thus bypassing the problem of singularities that can arise when the target is defined as the simple projection of the real vehicle on the path. The original formulation for wheeled ground robots can be found in Lapierre, Soetanto, and Pascoal (2003), and its application to AUVs, combined with backstepping control design methodologies, is presented in Lapierre and Soetanto (2007). A preliminary experimental validation for USVs was presented in Bibuli, Caccia, and Lapierre (2007). On the other hand, the approach introduced in Indiveri, Zizzari, and Mazzotta (2007) and experimentally validated with a testbed USV in Bibuli, Bruzzone, Caccia, Indiveri, and Zizzari (2008) explicitly addresses the underactuation of the vehicle already when defining the error variable to be globally and robustly stabilized to zero. Path follower performances can be enhanced by using preview controller design techniques as introduced in Gomes, Silvestre, Pascoal, and Cunha (2006). The role of the guidance system, computing all the reference signals needed to make the physical system autonomous, as well as the need for developing the guidance theory at the kinematic level in order to make it as general as possible, are discussed in Breivik and Fossen (2004). Using the path tangential speed as a virtual input, the along-track error is stabilized and uniform global exponential stability of the origin is proved in the case of unlimited speed. Moreover, a parameter adaptation technique to introduce integral action is proposed for environmental disturbance compensation.

According to the requirement of designing a generic path-following system, the application to a small autonomous catamaran, the Charlie USV, will be discussed in the sequel, pointing out the integration with the vehicle navigation and control system and the design and implementation of heuristics able

to increase performances on the basis of experimental results. In particular, a kinematic guidance law, generating a proper yaw-rate reference signal to drive the vehicle above the path, is combined with an already-implemented proportional integral (PI)-type velocity control level. On the other hand, some heuristic laws are introduced to face the problem of surge speed adaptation in function of the path curvature and steering action prediction. The surge speed reference value is modulated in a range of preset values in order to speed up the convergence to the required heading and to maintain the vehicle on the path when the path curvature increases.

The paper is organized as follows: In Section 2 the vehicle kinematics is described, both in free space and referred to the path-following task. A brief overview of an operational model of the Charlie USV dynamics is also presented. Section 3 discusses the proposed path-following guidance algorithm together with its relations with the system navigation, guidance and control architecture, and basic implementation issues. A couple of heuristic speed adaptation laws able to increase system performance are introduced too. The Charlie USV is presented in Section 4, and experimental results are reported and discussed in Section 5.

2. MODELING

2.1. General Kinematics

Assuming that the vessel motion is restricted to the horizontal plane, i.e., neglecting pitch and roll, two reference frames are considered: an inertial, earth-fixed frame $\langle e \rangle$, where position and orientation $[x \;\; y \;\; z]^T$ of the vessel are usually expressed, and a body-fixed frame $\langle b \rangle$, where surge and sway velocities ($[u \;\; v]^T$ absolute, $[u_r \;\; v_r]^T$ with respect to the water), yaw rate r, and forces and moments $[X \;\; Y \;\; N]^T$ are represented.

Denoting with $[\dot{x}_C \;\; \dot{y}_C]^T$ the sea current, supposed to be irrotational and constant, i.e., $\ddot{x}_C = \ddot{y}_C = 0$, the vehicle kinematics is usually modeled with the following equations, which are expressed in the earth-fixed frame:

$$\begin{aligned} \dot{x} &= u_r \cos\psi - v_r \sin\psi + \dot{x}_C, \\ \dot{y} &= u_r \sin\psi + v_r \cos\psi + \dot{y}_C, \\ \dot{\psi} &= r. \end{aligned} \tag{1}$$

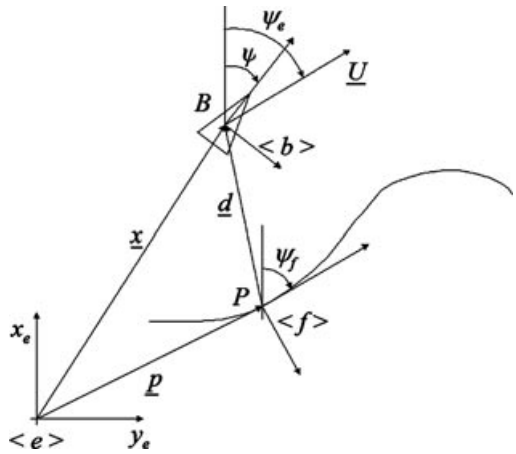

Figure 1. Vehicle parameters and frame definition.

Assuming that the vessel is moving at constant surge with respect to the water with negligible sway, i.e., $v_r = 0$ and $\dot{u}_r = \dot{v}_r = 0$, as in the case of the Charlie USV, the kinematic model (1) can be rewritten in terms of the total velocity as follows:

$$\begin{aligned} \dot{x} &= U \cos\psi_e, \\ \dot{y} &= U \sin\psi_e, \\ \dot{\psi}_e &= r\left[\frac{u_r^2}{U^2} + \frac{u_r}{U^2}(\dot{x}_C \cos\psi + \dot{y}_C \sin\psi)\right] = r\eta(t), \end{aligned} \tag{2}$$

where

$$\begin{aligned} U &= \sqrt{\dot{x}^2 + \dot{y}^2}, \\ \psi_e &= \arctan\frac{\dot{y}}{\dot{x}} \end{aligned}$$

denote the module and orientation of the vehicle speed in the earth-fixed reference frame $\langle e \rangle$. It is worth noting that the rotation rate of the vehicle speed orientation in the frame $\langle e \rangle$ is a function of a time variable parameter $\eta(t)$, inducted by sea currents, as shown by the third equation (2).

A graphical representation of the nomenclature of the USV kinematics is given in Figure 1, where variables describing the path-following problem are also pointed out.

2.2. Path-Following Kinematics

A Serret–Frenet frame $\langle f \rangle$, which moves along the path to be followed by the vehicle, is defined. Such a frame is usually called a *virtual target vehicle*, and it should be tracked by the *real vehicle*. With reference to Figure 1, P is an arbitrary point on the path, $\langle f \rangle$ is the Serret–Frenet frame associated to that point, and $\mathbf{p} = [x_P \;\; y_P \;\; 0]^T$ is the position vector of the point P with reference to the earth-fixed frame $\langle e \rangle$. The point B, attached to the vehicle body, can be expressed either as $\mathbf{x} = [x \;\; y \;\; 0]^T$ in $\langle e \rangle$ or as $[s_1 \;\; y_1 \;\; 0]^T$ in $\langle f \rangle$.

The rotation matrix from $\langle e \rangle$ to $\langle f \rangle$, parameterized locally by the angle ψ_f, which is the tangent to the path at point P, is denoted by

$$R = \begin{bmatrix} \cos\psi_f & \sin\psi_f & 0 \\ -\sin\psi_f & \cos\psi_f & 0 \\ 0 & 0 & 1 \end{bmatrix}.$$

Defining $r_f = \dot{\psi}_f$, and denoting with s the signed curvilinear abscissa along the path, the following expressions hold:

$$\begin{aligned} r_f &= \dot{\psi}_f = c_c(s)\,\dot{s}, \\ \dot{c}_c(s) &= g_c(s)\,\dot{s}, \end{aligned}$$

where $c_c(s)$ and $g_c(s) = dc_c(s)/ds$ denote the path curvature and its derivative, respectively.

The velocity of P in the Serret–Frenet frame $\langle f \rangle$ and the velocity of B in the earth-fixed frame $\langle e \rangle$ are, respectively,

$$\left(\frac{\mathrm{d}\mathbf{p}}{\mathrm{d}t}\right)_f = \begin{bmatrix} \dot{s} \\ 0 \\ 0 \end{bmatrix}$$

and

$$\begin{aligned} \left(\frac{\mathrm{d}\mathbf{x}}{\mathrm{d}t}\right)_e = \left(\frac{\mathrm{d}\mathbf{p}}{\mathrm{d}t}\right)_e + R^{-1}\left(\frac{\mathrm{d}\mathbf{d}}{\mathrm{d}t}\right)_f \\ + R^{-1}([0 \;\; 0 \;\; r_f]^T \times \mathbf{d}), \end{aligned}$$

where $\mathbf{d}$ is the vector from P to B.

The velocity of B in $\langle e \rangle$ expressed in $\langle f \rangle$, obtained by premultiplying the above equation by R, is

$$\begin{aligned} \left(\frac{\mathrm{d}\mathbf{x}}{\mathrm{d}t}\right)_f = R\left(\frac{\mathrm{d}\mathbf{x}}{\mathrm{d}t}\right)_e = \left(\frac{\mathrm{d}\mathbf{p}}{\mathrm{d}t}\right)_f + \left(\frac{\mathrm{d}\mathbf{d}}{\mathrm{d}t}\right)_f \\ + [0 \;\; 0 \;\; r_f]^T \times \mathbf{d}. \end{aligned} \tag{3}$$

Using the relations

$$\left(\frac{\mathrm{d}\mathbf{x}}{\mathrm{d}t}\right)_e = \begin{bmatrix} \dot{x} \\ \dot{y} \\ 0 \end{bmatrix},$$

$$\left(\frac{\mathrm{d}\mathbf{d}}{\mathrm{d}t}\right)_f = \begin{bmatrix} \dot{s}_1 \\ \dot{y}_1 \\ 0 \end{bmatrix},$$

and

$$[0 \;\; 0 \;\; r_f]^T \times \mathbf{d} = \begin{bmatrix} 0 \\ 0 \\ c_c(s)\,\dot{s} \end{bmatrix} \times \begin{bmatrix} s_1 \\ y_1 \\ 0 \end{bmatrix} = \begin{bmatrix} -c_c(s)\,\dot{s}\,y_1 \\ c_c(s)\,\dot{s}\,s_1 \\ 0 \end{bmatrix},$$

Eq. (3) can be rewritten as

$$R\begin{bmatrix} \dot{x} \\ \dot{y} \\ 0 \end{bmatrix} = \begin{bmatrix} \dot{s}[1 - c_c(s)y_1] + \dot{s}_1 \\ \dot{y}_1 + c_c(s)\,\dot{s}\,s_1 \\ 0 \end{bmatrix}.$$

Solving for $\dot{s}_1$ and $\dot{y}_1$ yields

$$\begin{aligned} \dot{s}_1 &= [\cos\psi_f \quad \sin\psi_f]\begin{bmatrix} \dot{x} \\ \dot{y} \end{bmatrix} - \dot{s}(1 - c_c y_1), \\ \dot{y}_1 &= [-\sin\psi_f \quad \cos\psi_f]\begin{bmatrix} \dot{x} \\ \dot{y} \end{bmatrix} - c_c\,\dot{s}\,s_1. \end{aligned} \tag{4}$$

Finally, replacing the top two equations (2) in Eqs. (4) and introducing the variable $\beta = \psi_e - \psi_f$ gives the *kinematic* model of the vehicle in (s, y) coordinates as

$$\begin{aligned} \dot{s}_1 &= -\dot{s}(1 - c_c y_1) + U\cos\beta, \\ \dot{y}_1 &= -c_c\dot{s}s_1 + U\sin\beta, \\ \dot{\beta} &= r_e - c_c\dot{s}, \end{aligned}$$

where $r_e = \dot{\psi}_e = r\eta(t)$.

2.3. Dynamics

As mentioned in Section 1, the work presented in this paper focuses on the design of a path-following guidance law at the kinematic level, while the generated reference yaw rate is tracked by a low-level dedicated controller already present on the test bed USV. In particular, the Charlie USV is equipped with model-based linear and angular velocity controllers, as well as motion estimators. Thus, a brief discussion of the adopted model of the vehicle dynamics is reported

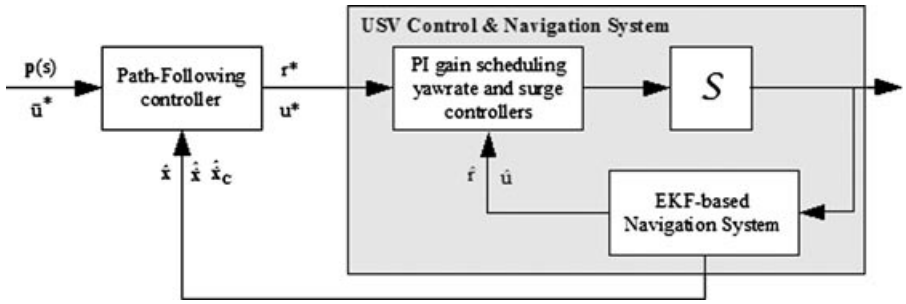

Figure 2. Dual-loop navigation, guidance, and control architecture.

in the following. For a detailed discussion of the assumptions and experimental results that led to the definition of a *practical* model[2] for the Charlie USV dynamics, the reader can refer to Caccia, Bruzzone, and Bono (2008). In particular, because the vessel speed with respect to the water is about proportional to the propeller revolution rate, experiments carried out with the Charlie USV revealed the impossibility of observing both of these quantities, as well as sway dynamics, using measurements only from onboard global positioning system (GPS) and compass. Thus, sway speed can be neglected and the dynamics can be reduced to

$$\tilde{m}_u \dot{u}_r = \tilde{k}_u u_r + \tilde{k}_{u_r^2} u_r^2 + \tilde{k}_{n^2\delta^2} n^2 \delta^2 + n^2, \tag{5}$$

$$\tilde{I}_r \dot{r} = \tilde{k}_r r + \tilde{k}_{r|r|} r|r| + \tilde{k}_{n^2} n^2 + n^2 \delta, \tag{6}$$

where n is the propeller revolution rate; δ is the rudder angle; $\tilde{m}_u$ and $\tilde{I}_r$ are the normalized inertia terms; $\tilde{k}_u$, $\tilde{k}_{u_r^2}$, $\tilde{k}_r$, and $\tilde{k}_{r|r|}$ are the drag coefficients; $\tilde{k}_{n^2\delta^2}$ represents the resistance due to the rudder; and $\tilde{k}_n^2$ takes into account the vessel longitudinal asymmetries.

Because, as discussed above, in Eq. (6) the steering torque $n^2\delta$ has been identified as a function of the propeller revolution rate instead of the advance speed, the rudder action is neglected when the vehicle is still moving while n is zero. Thus, it is worth noting that the field of validity of the proposed model of vehicle dynamics is for $n > \bar{n} > 0$. As remarked in Section 3.3, this forces a minimum USV speed for guaranteeing maneuvering capabilities.

[2]*Practical* stands for consistent, from the point of view of degree of accuracy, quality in terms of noise and sampling rate of the measurements.

3. GUIDANCE AND CONTROL

3.1. Navigation, Guidance, and Control Architecture

A dual-loop hierarchical guidance and control architecture decoupling kinematics and dynamics is adopted. In the proposed control scheme, the external guidance loop performs position control, generating suitable velocity references according to the desired task, i.e., path following in this case. The dynamic controllers have to ensure that the actual rotational and linear speed of the vehicle tracks the references with sufficient precision to guarantee the overall stability of the system. Although a rigorous demonstration of system stability is not given, the design of guidance task functions at the kinematic level is usually very simple, as are the tuning of the kinematic and dynamic controller parameters on the basis of empirical considerations as discussed in Caccia (2007) and Caccia, Bibuli, Bono, and Bruzzone (2008).

As shown in Figure 2, this architecture implements different motion task functions while keeping unchanged the vehicle control and navigation system. In the case of the Charlie USV, a navigation system relying on model-based extended Kalman filters estimates the vessel position $\boldsymbol{x}$, orientation and speed $\dot{\mathbf{x}}$, as well sea current velocity $\dot{\mathbf{x}}_C$, in the earth-fixed frame $\langle e \rangle$ and surge u and yaw rate r in the body-fixed frame $\langle b \rangle$. PI-type linear and angular velocity controllers are designed following a gain-scheduling approach in order to guarantee a specific behavior, in terms of closed-loop characteristic equations. A detailed discussion of the Charlie USV navigation and control system can be found in Caccia, Bibuli, et al. (2008). Here, it is sufficient to point out that the kinematic path-following guidance law, computed as discussed in Section 3.2, feeds a lower

level PI-type yaw-rate dynamic controller. Although the proof of stability of the overall dual-loop control scheme is not considered in this paper, the kinematic controller parameters are assumed to be set such that the rate of change of the reference yaw rate r^* is slow enough to be perfectly tracked by the dynamic controller.

3.2. Kinematic Controller Design

Usually, the solution to the path-following problem is based on the zeroing of the distances between the vehicle and a point P on the path and the angle β between the vehicle's total velocity vector U and the tangent to the path at P. With respect to classical approaches in which P is the closest point on the path, the key idea proposed in this paper is to consider the target point, with its associated Serret–Frenet frame $\langle f \rangle$, moving along the path according to a defined control law, obtaining in this way an extra controller design parameter.

As discussed in Lapierre and Soetanto (2007), the demonstration of stability of the proposed controller is essentially based on the application of Barbalat's lemma and LaSalle's theorem.

Because the application of LaSalle's theorem is restricted to autonomous systems, in the examined case the fact that the desired forward velocity is a constant allows the system to be considered autonomous. In the following, a trace of the main steps in designing the Lyapunov-based controller is given. For a rigorous proof the reader can refer to Lapierre and Soetanto (2007).

First a desired approach angle φ is defined as a function of the distance of the USV from the tangent line to the path in the point P, i.e., y_1 in the Serret–Frenet frame $\langle f \rangle$. The function $\varphi(y_1)$ has to satisfy the constraints $\|\varphi(y_1)\| < \pi/2$, $y_1\varphi(y_1) \leq 0$, and $\varphi(0) = 0$, stating that the vehicle heads for the desired path and remains over it once reached.

For instance, the following hyperbolic tangent–shaped function, parameterized by $k_\varphi > 0$ and $0 < \psi_a < \pi/2$, with its saturation properties satisfies the above-mentioned requirements:

$$\varphi(y_1) = -\psi_a \tanh(k_\varphi y_1). \tag{7}$$

Then, the vehicle approach angle β is imposed to track the desired one, φ, by considering the candidate Lyapunov function

$$V = \tfrac{1}{2}(\beta - \varphi)^2.$$

Its time derivative

$$\dot{V} = (\dot{\beta} - \dot{\varphi})(\beta - \varphi) = [r\,\eta(t) - c_c\,\dot{s} - \dot{\varphi}](\beta - \varphi)$$

is negative-semidefinite, $\dot{V} = -k_1(\beta - \varphi)^2$, when choosing the control law

$$r^* = \frac{1}{\eta(t)}[\dot{\varphi} - k_1(\beta - \varphi) + c_c(s)\,\dot{s}], \tag{8}$$

where $k_1 \geq 0$.

Because V is lower bounded and $\dot{V}$ is uniformly continuous, Barbalat's lemma leads to the conclusion that $\lim_{t\to+\infty} \dot{V} = 0$.

Moreover, the proposed control law makes variables β, s_1, and y_1 bounded and approaching the set E, defined by $\dot{V} = 0$. The motion of the feedback control system, restricted to E, can be studied considering the Lyapunov function:

$$V_E = \tfrac{1}{2}\left(s_1^2 + y_1^2\right).$$

Computing its time derivative

$$\dot{V}_E = (U\cos\beta - \dot{s})s_1 + U y_1 \sin\beta,$$

it is worth noting that the speed $\dot{s}$ of the target Serret–Frenet $\langle f \rangle$ constitutes an additional degree of freedom that can be controlled in order to guarantee the convergence of the vehicle at the desired path. In particular, considering that, in the set E, $\beta = \varphi(y_1)$ and that $y_1 \sin\varphi(y_1) \leq 0$ for the choice of $\varphi(y_1)$, the control law

$$\dot{s}^* = U\cos\beta + k_2 s_1 \tag{9}$$

with $k_2 > 0$ guarantees $\dot{V}_E \leq 0$. Because $\ddot{V}_E$ is bounded, for Barbalat's lemma $\lim_{t\to+\infty} \dot{V}_E = 0$, which in turn implies that all trajectories in E satisfy $\lim_{t\to+\infty} s_1 = 0$ and $\lim_{t\to+\infty} y_1 = 0$. Thus the asymptotic convergence to zero of the variables β, s_1, and y_1 is guaranteed.

The controller exposed in Eq. (8) with the virtual target equation of motion (9) has been implemented on the Charlie USV's architecture. Experimental results are reported in Section 5. The advantages

of the proposed controller are summarized as follows:

- The nonlinear approach angle φ [see Eq. (7)], originally introduced by C. Samson (Micaelli & Samson, 1993), allows for driving the incidence angle of the robot with respect to path. Indeed when y_1 is high, the desired incidence is $\pm\psi_a$, i.e., $\pm\pi/2$, that is, the vehicle's orientation is driven perpendicularly to the path tangent. As y_1 reduces, the incidence also reduces, and it vanishes to zero as y_1 is zero, i.e., when the vehicle is on the path.
- The virtual target principle, denoted as $\dot{s}$, introduces an extra (and virtual) degree of freedom to the system. Controlling the virtual target as expressed in Eq. (9) removes the classic singularity of the path-following problem exposed in Micaelli and Samson (1993). Indeed, the consideration of the closest point on the path as the target to be tracked by the vehicle imposes a severe limitation in the domain of attraction of the control. The virtual target allows for enlarging this domain of attraction to the whole space, thus removing singularity.

Sea current compensation. As discussed in Caccia, Bibuli, et al. (2008), where the case of straight line following was addressed, lateral sea currents are naturally compensated by guidance laws generating a reference yaw rate as a function only of the range from the target path and its first derivative. Indeed, thanks to an integrator embedded in the kinematics of the linearized physical system around the equilibrium point, the vehicle naturally heads in such a way of following the desired line while compensating lateral sea current. This property, which guarantees local stability, is not valid when the reference yaw rate is somehow computed as a function of a desired heading angle. In this case, the presence of neglected constant sea current disturbances yields a steady-state error in the range from the desired path.

Because the measurement of sea current is not always available onboard small USVs, and its estimate can be very imprecise or noisy, operating conditions can require the adoption of guidance laws neglecting this class of disturbances. How neglecting sea current affects the proposed path-following guidance law is discussed in the following.

In Eq. (8) the term $\eta(t) = [u_r^2/U^2 + u_r/U^2 (\dot{x}_c \cos\psi + \dot{y}_c \sin\psi)]$ can be unknown or roughly estimated. Adding some practical constraints, the multiplicative noise term could be neglected. Indeed, considering the typical operative conditions in which the vehicle surge with respect to the water is higher than the sea current,

$$\sqrt{\dot{x}_C^2 + \dot{y}_C^2} < u_r,$$

the *noise* function $\eta(t)$ is always positive and never reaches the zero value.

So, assuming $\eta(t) = 1$, i.e., neglecting sea currents, and rewriting the guidance law for r as

$$r^* = \dot{\varphi} - k_1(\beta - \varphi) + c_c(s)\,\dot{s},$$

the derivation of V yields

$$\dot{V} = -k_1\eta(t)(\beta - \varphi)^2 + (\eta - 1)(\dot{\varphi} + c_c\,\dot{s})(\beta - \varphi),$$

which is negative outside of the interval limited by zero and $\frac{\eta(t)-1}{k_1\eta(t)}(\dot{\varphi} + c_c\dot{s})$, which defines a tube around the path that the system is guaranteed to reach.

Behavior at path beginning and end. The desired path has typically a beginning and an end, i.e., is typically defined for constrained values of the curvilinear abscissa. Thus, the evolution of s according to Eq. (9) has to be constrained in the interval $s \in [0\ \ s_{\mathrm{MAX}}]$. In particular, forcing s to 0 or s_{MAX} when its evolution would lead it outside of the desired interval is equivalent to forcing the vehicle to follow the tangent to the path at its beginning or end point, respectively. From a practical point of view, this is usually not dangerous when the vehicle approaches the path starting point along its tangent. On the other hand, a vehicle that tries to move along the path tangent after its end can be very dangerous. So, safety maneuvers, e.g., rotating at constant yaw rate, have to be executed when the vehicle reaches the end of the path, i.e., $s^* = s_{\mathrm{MAX}}$.

Generic path software representation. The issue of generic representation of paths in the software implementation has been addressed too. Although only explicit representations through mathematical functions can guarantee exact computation of the path properties for every value of the curvilinear abscissa s, from the point of view of software implementation such an approach would limit the possible paths to a set of classes of functions known by the system. Thus, a generic path is represented as a sequence of points, discretized for $s = s_0, \ldots, s_N = s_{\mathrm{MAX}}$, with the

corresponding tangent vector and curvature. For intermediate values of s, the path parameters are linearly interpolated: $p(s) = p(s_i) + \frac{p(s_{i+1}) - p(s_i)}{s_{i+1} - s_i}(s - s_i)$ for $s \in (s_i, s_{i+1})$, where p can represent the path point coordinates, tangent vector components, or curvature.

3.3. Heuristic Speed Adaptation

The above-discussed guidance law drives an ideal vessel with no leeway with respect to the water over a desired path. Indeed, the actual test bed USV is characterized by physical limitations on the maximum yaw rate and unmodeled sway with respect to the water. The result is that the vehicle, when working at constant surge, can execute large U-turns for heading the path or sliding away from the path when executing sharp curves.

The proposed solution to this issue arises from human common behavior when driving a vehicle: while approaching a curve or when tricky maneuvers are needed, advance speed is reduced with respect to the desired $\bar{u}^*$ established by the human operator or mission controller.

Assuming that the vehicle speed is within a minimum $U_{\min}$, needed to allow maneuvering capabilities (see Section 2.3 for details) and a maximum $U_{\max}$, a heuristic law has been introduced in the global regulation schema to improve the guidance and control system performances.

From this concept arise the equations that model such a behavior: first, an adaptation for the maximum surge speed is computed as a function of the actual yaw rate requested by the controller:

$$u^*_{1_{\mathrm{MAX}}} = \frac{U_{\max} - U_{\min}}{2} + \frac{U_{\max} - U_{\min}}{2}\left[\cos\left(\frac{\pi r^*}{r_{\mathrm{sat}}}\right)\right], \tag{10}$$

where $U_{\max}$, $U_{\min}$, and r_{sat} are parameters of the adaptation law. This reduces surge speed when the vehicle orientation is far from the required heading in order to speed up the convergence to the desired approach angle. Thus, a second adapted maximum reference surge speed is computed on the basis of a prediction of the maximum curvature of the path inside a predefined prediction horizon:

$$u^*_{2_{\mathrm{MAX}}} = U_{\min} + (U_{\max} - U_{\min})[1 - \tanh^2(k_u c_{\max})], \tag{11}$$

where k_u is a free parameter and $c_{\max}$ is the maximum value of $c_c(\bar{s})$, with $\bar{s}$ in $[s; s + h]$, and h is the prediction horizon. This helps the vehicle to maintain its position above high-curvature segments of the path. Finally, the adapted maximum reference surge speed is computed as the minimum between $u^*_{1_{\mathrm{MAX}}}$ and $u^*_{2_{\mathrm{MAX}}}$:

$$u^*_{\mathrm{MAX}} = \min\left(u^*_{1_{\mathrm{MAX}}}, u^*_{2_{\mathrm{MAX}}}\right)$$

and the adapted reference surge is

$$u^* = \min\left(\bar{u}^*, u^*_{\mathrm{MAX}}\right).$$

The reader should note that expression (10) contains the control input r^*, thus introducing a coupling between the yaw and surge control inputs. The authors are aware of the algebraic loop introduced by this method. Nevertheless, note that this coupling will induce a reduced surge velocity. The improvement of this method is clearly exposed in Section 5, where experimental results validate the proposed approach.

4. CHARLIE USV

The Charlie USV (see Fig. 3) is a small catamaran-shape-like prototype vehicle, originally developed and exploited, during the XIX Italian expedition to Antarctica in 2003–2004, by the CNR–ISSIA for the sampling of the sea surface microlayer and immediate subsurface for the study of the sea–air interaction (Caccia et al., 2005). Charlie is 2.40 m long and 1.70 m wide and weighs about 300 kg in air. The propulsion system of the vehicle is composed of a couple of dc motors (300 W at 48 V), with a set of servoamplifiers that provide a PID control of the propeller revolution rates. In the current release, the vehicle is equipped with a rudder-based steering system, where two rigidly connected rudders, positioned behind the thrusters, are actuated by a brushless dc motor. The navigation instrumentation set is constituted of a GPS Ashtech GG24C integrated with a KVH Azimuth Gyrotrac able to compute true north. Electrical power supply is provided by four 12 V at 40 Ah lead batteries integrated with four 32-W triple junction flexible solar panels. The onboard real-time control system, developed in C++, is based on GNU/Linux and run on a single board computer (SBC), which supports serial and Ethernet communications and PC-104 modules for digital and analog input/output (I/O) (Bruzzone, Caccia, Bertone, & Ravera, 2008). An overview of the Charlie project, including a detailed description of the vehicle and a

Figure 3. The Charlie USV.

summary of its applications, can be found in Caccia et al. (2007). Nominal values for the parameters of the Charlie USV dynamics, as modeled in Eqs. (5) and (6), can be found in Caccia, Bruzzone, et al. (2008).

5. EXPERIMENTS: METHODOLOGY AND RESULTS

Experimental tests have been carried out in the Genova Prà harbor (see Figure 4), a calm water channel devoted to rowing races; the site is usually beaten by a 20–30-kn wind. Results obtained during a preliminary session of trials, carried out in December 2006, are reported and discussed in Bibuli et al. (2007), where the integration with backstepping techniques for handling the vehicle dynamics has been considered too. The tests discussed in the following were performed in winter 2008–2009 in calm wind conditions.

The field trials had two basic goals:

(i) proving the practical validity of the proposed theoretical guidance laws (8) and (9); and
(ii) evaluating the benefits given by the heuristic speed adaptation rules, which force a speed reduction when turning and anticipating significant path curvature.

A set of metrics was defined for measuring the capability of the vehicle to follow the desired path. In particular, the performance of the guidance system in steady state is measured by the area between the actual and the reference paths, normalized with respect to the path length. This quantity, together with the evaluation of the maximum distance y_1 from the target path, allows a quantitative evaluation of the practical validity of the proposed approach as well as of the effects of adaptive speed control on the basis of the predicted path curvature. On the other hand, field experience, pointing out the practical difficulties in executing repetitive experiments at sea, suggested the execution of a set of trials with the vehicle following a straight line. In particular, homogeneous initial conditions were guaranteed by simply inverting the direction of the target line while the vehicle was tracking it in steady state. The evaluation of the benefits obtained by reducing speed when turning is clear in these experimental conditions. Thus, as shown in Figure 5, the USV maneuver is divided into three phases:

1. *U-turn*, or more generally speaking, *path approach*, while the vehicle reaches (and eventually crosses) the target path. This phase starts at the end of the previous maneuver,

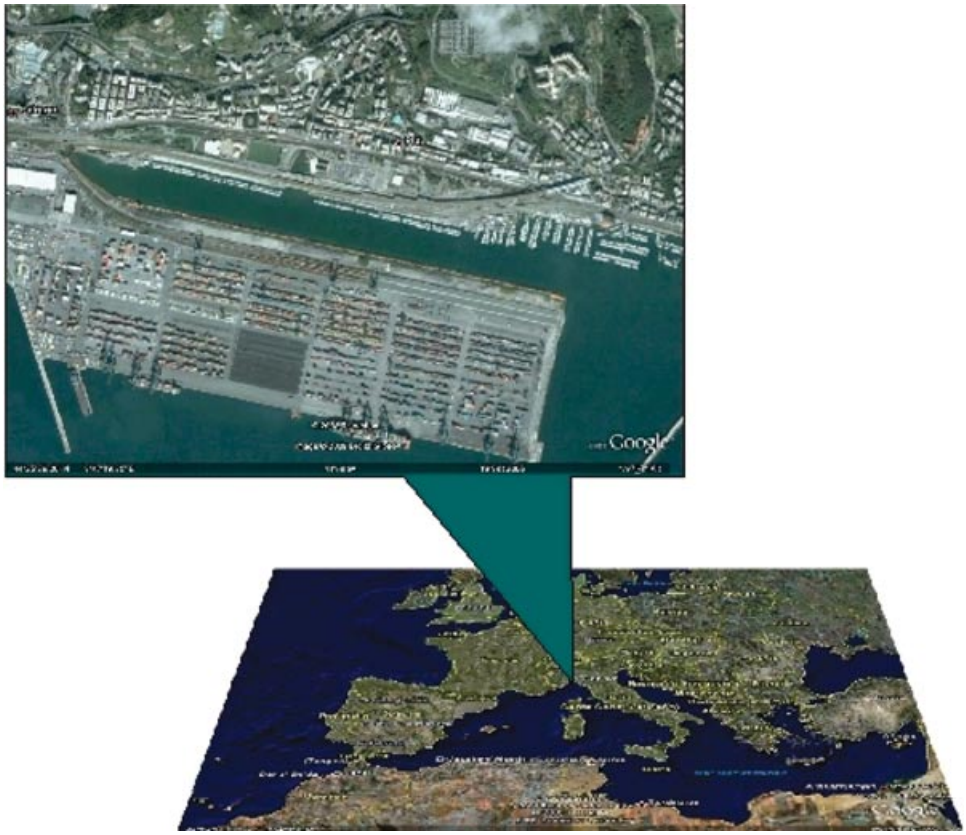

Figure 4. Genova Prà test site (Google Earth view).

indicated as instant E, and terminates with the crossing of the target path, denoted as instant T, i.e., the beginning of the *transient*. The quantities $L_{\parallel}$ and $L_{\perp}$, as well as the area $A_{\text{U-turn}}$ between the actual path and the desired line, measure the vessel maneuvering space for executing a U-turn.

2. *Transient*, while the vehicle reaches steady-state conditions. The settling instant, when the vehicle enters steady state, is denoted by S. During this phase, if present, the *overshoot* is measured.
3. *Steady state*, while the vehicle motion stabilizes around a straight line parallel to the desired one (almost constant external disturbance could induce a range error from the reference track). This phase ends when a new maneuver is set. The precision of the guidance system is measured by the quantity $\bar{A}_{\text{ss}} = A_{\text{ss}}/\Delta s_{\text{ss}}$, where A_{ss} represents the area between the actual path and the desired line and $\Delta s_{\text{ss}} = s(E_i) - s(E_{i-1})$ is the path length in steady-state conditions during the ith maneuver.

It is worth noting that, for the purpose of this research, the settling time, when following a straight line, has been automatically determined in post-processing as follows. Denoting with $\bar{y}_{1_t} = \frac{\int_t^{E_i} y_1(\tau)d\tau}{E_i - t}$ the mean value of y_1 from the target line from a given time t and the end of the current maneuver E_i, and with $\text{std}(y_{1_t})$ its standard deviation, S_i is the maximum value of t such that $|\bar{e}_t| \leq \max\{k\text{std}(y_{1_t}), e_{\min}\}, \forall \tau \in [t, , E_i]$ with k and $e_{\min}$ suitable positive constants.

In this context, the kinematic guidance algorithm, with different approach angles, has been tested without speed adaptation and with the guidance law integrated with the speed adaptation heuristic, accomplishing dynamic control with the Charlie USV

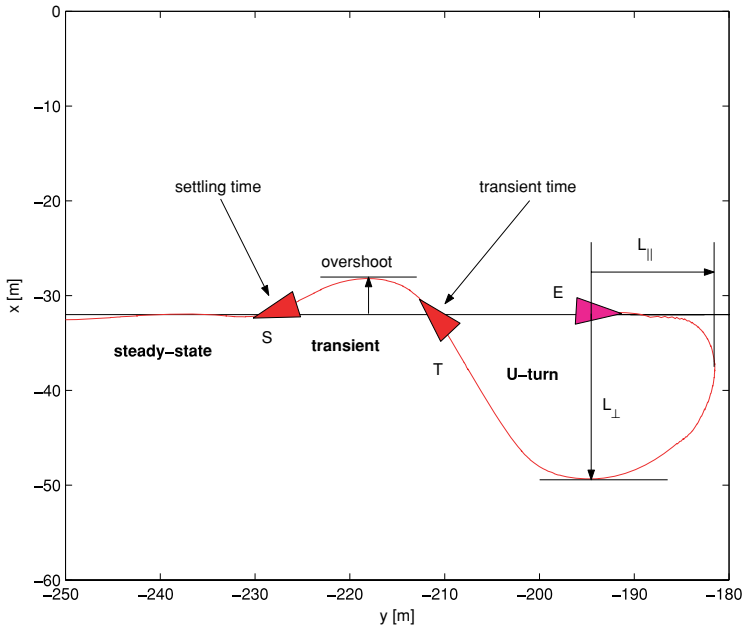

Figure 5. Metrics adopted for quantitatively evaluating path-following guidance system performance (nomenclature).

standard PI gain-scheduling, yaw-rate controller. The vehicle navigation system consisted of conventional extended and linear time-varying Kalman filters processing GPS and compass measurements. Experimental identification of the vehicle dynamics allowed the open-loop estimate of its surge speed with respect to the water, on the basis of the normalized propeller revolution rate and rudder deflection by online integrating equation (5). This operation is equivalent to implementing a kind of virtual velocity sensor consisting of an open-loop, model-based predictor in the manner presented in Caccia and Veruggio (1999). For a detailed discussion of the Charlie USV navigation and control system, the reader can refer to Caccia, Bibuli, et al. (2008). The desired path was specified through a suitable graphical user interface, which allowed the operator to supervise the vehicle behavior during the tests (see Figure 6). Experiments with the Charlie USV following a straight line in alternate directions demonstrated the benefits obtained by adapting the surge speed in a function of the actual yaw rate requested by the controller.

As in all the other experiments presented in this paper, the USV reference surge was set to 1 m/s, and its minimum value was fixed at 0.6 m/s in order to guarantee a smooth maneuverability of the vehicle. The gains k_1 and k_2 of the steering and virtual target speed control laws were assumed equal to 0.2 and 1.0, respectively. The hyperbolic tangent of the approach angle was shaped by the parameter $k_\varphi = 0.3$.

To validate the guidance system behavior while executing straight line following with different approach angles, tests were performed for three values of the parameter ψ_a, i.e., 30, 60, and 90 deg, respectively, both with standard algorithm and adopting speed adaptation. In particular, in the case when speed adaptation was not activated, six experiments were carried out with the Charlie USV for each angle of approach. As shown in Figure 7, the parameters characterizing the U-turn maneuver were not computed for test number 1 because in that case the vehicle approached the target line from a far point. On the other hand, seven U-turn maneuvers for $\psi_a = 60$ and 30 deg and six for $\psi_a = 90$ deg, respectively, were executed in the case when speed adaptation was activated. The proposed guidance law demonstrated its capability in managing inversions of direction in following a line without any singularity.

The computed values of the metrics characterizing the maneuver performance of the USV when using the standard guidance law and the speed

Figure 6. Charlie graphical user interface while monitoring path following.

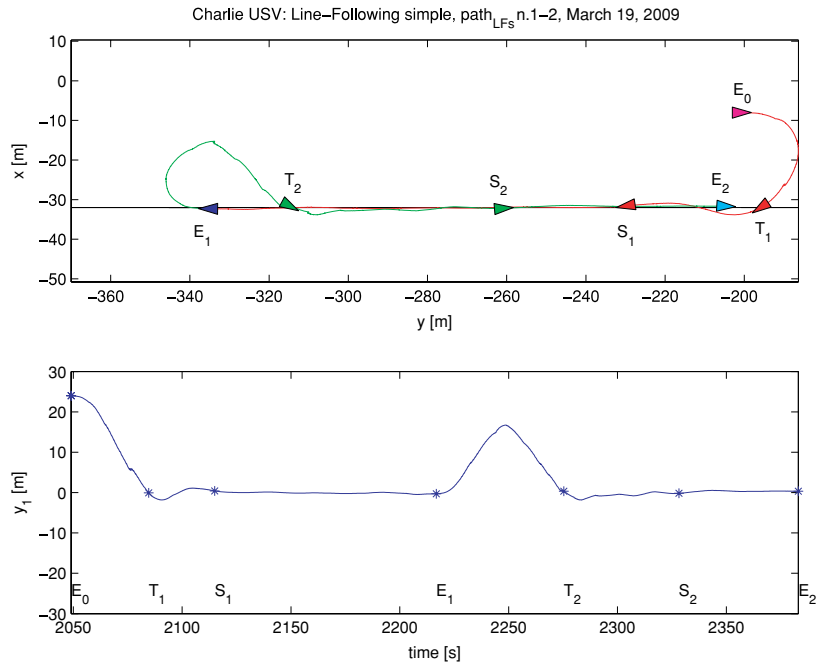

Figure 7. Charlie USV approaching a straight line and executing a U-turn: $\psi_a = 60$ deg. From top to bottom: actual vehicle path; range from the desired path y_1.

Table I. Performance metrics: Straight line following with no speed adaptation.

n	ψ_a (deg)	$L_\parallel$ (m)	$L_\perp$ (m)	$A_{\text{U-turn}}$ (m^2)	Overshoot (m)	$\bar{A}_{\text{ss}}$ (m)
1	60.00	—	—	—	1.83	0.15
2	60.00	10.62	17.04	313.58	1.84	0.33
3	60.00	10.71	16.80	321.95	3.39	0.30
4	60.00	11.42	19.72	400.25	2.47	0.14
5	60.00	12.24	17.59	373.86	3.81	0.17
6	60.00	11.34	12.75	128.40	0.43	0.31
7	30.00	13.29	19.97	521.82	0.75	0.23
8	30.00	16.26	21.41	675.40	0.00	0.14
9	30.00	16.66	23.34	789.54	0.00	0.17
10	30.00	10.79	20.36	603.35	0.00	0.20
11	30.00	13.20	18.46	503.67	0.66	0.14
12	30.00	11.20	19.86	582.76	0.00	0.12
13	90.00	27.13	14.76	338.63	7.90	0.12
14	90.00	30.06	9.38	279.69	3.07	0.15
15	90.00	25.61	15.17	394.89	6.05	0.18
16	90.00	28.20	10.59	335.29	4.41	0.14
19	90.00	30.91	16.79	293.79	3.12	0.15
20	90.00	14.78	21.67	571.62	1.54	0.21

Table II. Performance metrics: Straight line following with speed adaptation.

n	ψ_a (deg)	$L_\parallel$ (m)	$L_\perp$ (m)	$A_{\text{U-turn}}$ (m^2)	Overshoot (m)	$\bar{A}_{\text{ss}}$ (m)
1	60.00	9.48	9.19	114.42	0.00	0.10
2	60.00	7.87	7.46	52.77	1.76	0.15
3	60.00	7.68	8.71	68.17	0.00	0.10
4	60.00	7.60	8.78	66.46	1.11	0.18
5	60.00	7.15	7.74	55.44	0.72	0.13
6	60.00	10.89	9.25	102.90	0.94	0.12
7	60.00	10.47	9.98	130.91	0.56	0.15
8	30.00	11.73	9.49	168.20	0.00	0.25
9	30.00	8.76	9.68	182.57	0.00	0.15
10	30.00	5.55	10.38	176.17	0.00	0.29
11	30.00	8.86	8.03	106.84	0.00	0.20
12	30.00	10.65	9.80	185.70	0.00	0.20
13	30.00	7.02	9.09	125.26	0.00	0.34
14	30.00	9.50	9.68	178.39	0.00	0.08
15	90.00	7.84	7.14	56.45	—	1.04
16	90.00	4.17	8.88	63.35	—	0.73
17	90.00	15.16	5.85	52.58	—	0.86
18	90.00	8.94	7.28	41.21	—	1.26
19	90.00	7.53	7.04	68.91	—	1.76
20	90.00	7.58	10.30	71.30	—	0.96

adaptation are reported in Tables I and II, respectively. A view of the USV behavior in the different test cases is shown in Figure 8, where the reduced space of maneuver required when the speed adaptation algorithm is adopted is clearly visible.

From a quantitative point of view, the mean values of the parameters characterizing the U-turn maneuvering space are reported in Table III. A reduction of the linear dimensions by a factor of about 2 is pointed out, when the USV surge speed decreases with its yaw rate according to Eq. (10). Because the combination of reduced speed and orthogonal approach angle leads the system to a limit cycle with persistent oscillations around the desired path (see the bottom right-hand graphs of Figure 8), tests carried out with $\psi_a = 90$ deg have not been considered for evaluating system behavior during *transient* and *steady-state* conditions. Moreover, due to these oscillations, overshoot estimations cannot be evaluated and are not reported in Table II.

As far as the *transient* phase is concerned, considering that a nominal approach angle of 30 deg typically induces a negligible offset and that there are permanent oscillations in the presence of speed adaptation and $\psi_a = 90$ deg, the analysis is limited to the case of $\psi_a = 60$ deg. In these conditions, the mean value of the overshoot decreases from 2.39 to 0.73 m when rules for speed adaptation are applied.

Table III. Performance metrics: Straight line following, U-turn maneuver parameters.

	ψ_a (deg)	No speed adaptation	With speed adaptation
$E\{L_\parallel\}$ (m)	60.00	11.27	7.60
$E\{L_\parallel\}$ (m)	30.00	13.57	8.87
$E\{L_\parallel\}$ (m)	90.00	26.11	8.54
$E\{L_\perp\}$ (m)	60.00	16.78	8.73
$E\{L_\perp\}$ (m)	30.00	20.56	9.45
$E\{L_\perp\}$ (m)	90.00	14.73	7.75
$E\{A_{\text{U-turn}}\}$ (m^2)	60.00	307.61	84.44
$E\{A_{\text{U-turn}}\}$ (m^2)	30.00	612.76	160.45
$E\{A_{\text{U-turn}}\}$ (m^2)	90.00	368,98	58.97

The performance of the proposed guidance law in driving the Charlie USV along a generic path was

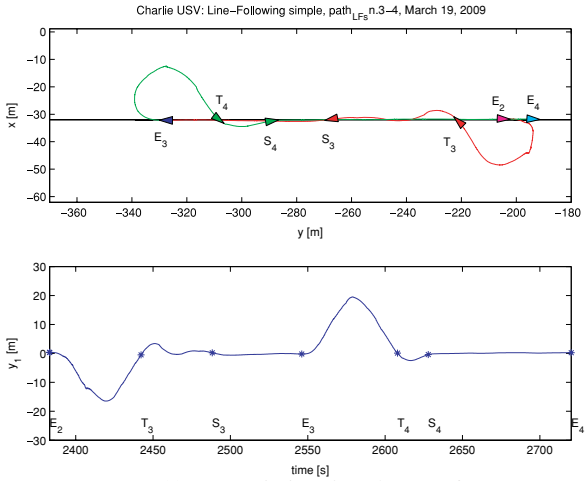

(a) No speed adaptation, $\psi_a = 60$ deg

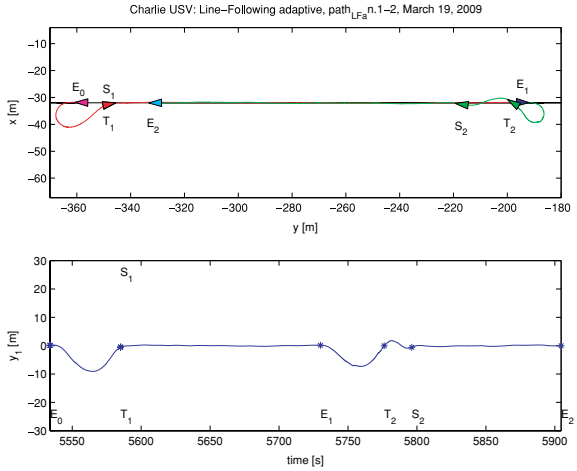

(b) With speed adaptation, $\psi_a = 60$ deg

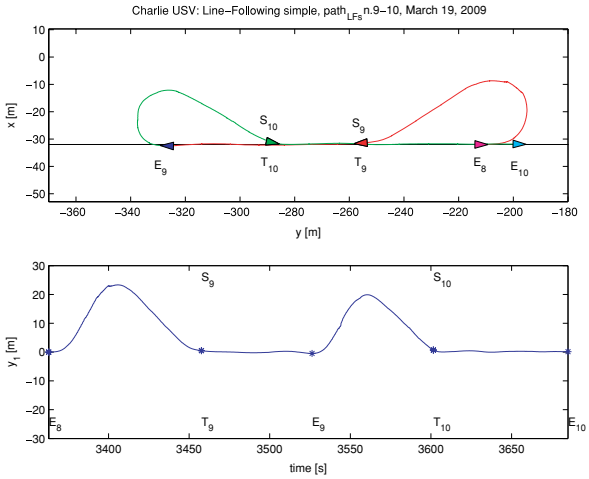

(c) No speed adaptation, $\psi_a = 30$ deg

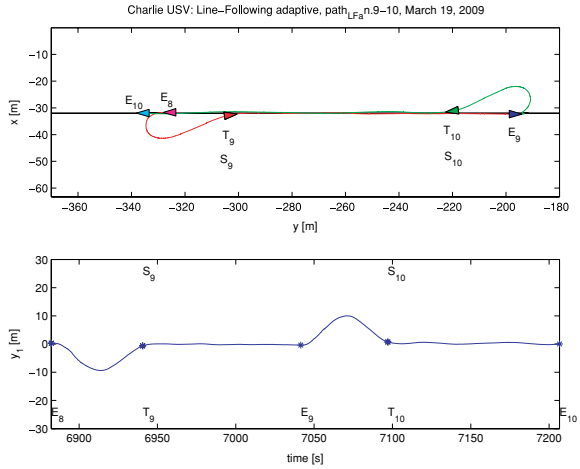

(d) With speed adaptation, $\psi_a = 30$ deg

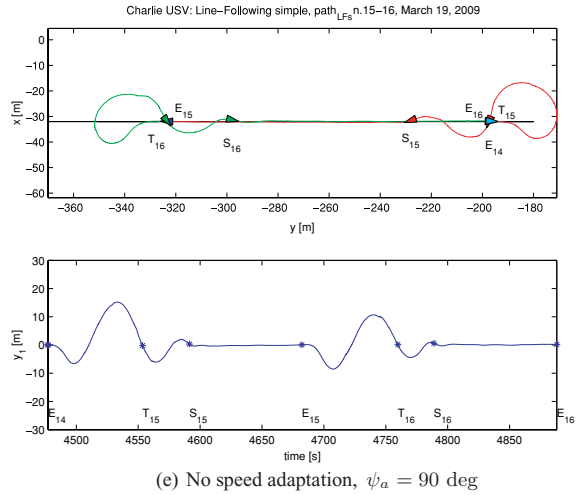

(e) No speed adaptation, $\psi_a = 90$ deg

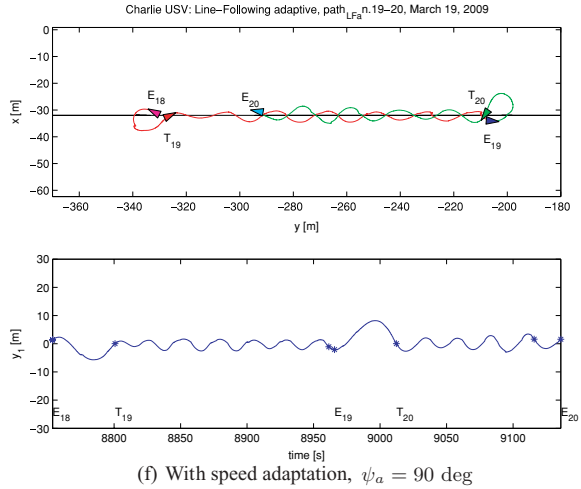

(f) With speed adaptation, $\psi_a = 90$ deg

Figure 8. Charlie USV straight line following.

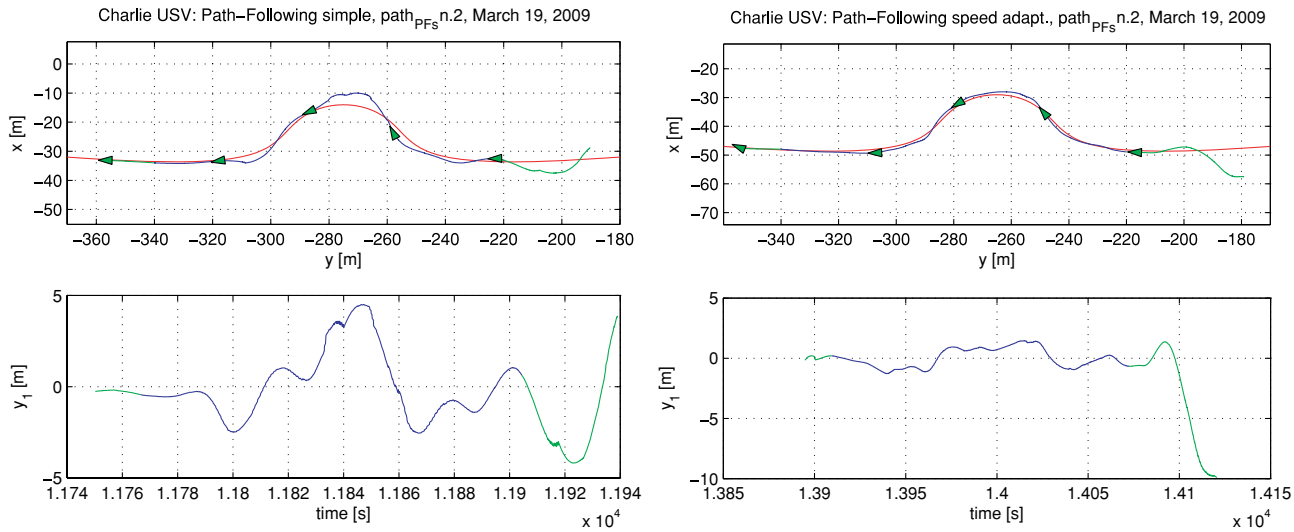

(a) No speed adaptation, $\psi_a = 60$ deg

(b) With speed adaptation, $\psi_a = 60$ deg

Figure 9. Charlie USV path following.

evaluated considering a bell-shaped path with curvature peaks equal to 0.045 in the midturn and to 0.047 in the side turns. The vehicle moved along the same path alternatively in the opposite directions, approaching it with an angle $\psi_a = 60$ deg. Three experiments were executed for each speed adaptation configuration. Examples of the vehicle path are shown in Figure 9, where the dramatic reduction of the maximum range from the desired path y_1, as a consequence of the adoption of the speed limitation rule (11), is pointed out. Results, i.e., the area between the actual and the desired paths, normalized with respect to the path length, are reported in Table IV. In Table V, the mean values of $\bar{A}_{ss}$, i.e., the normalized area between the actual and the desired paths in steady state, are reported for the above-mentioned experiments of generic path and straight line following. In the case of straight line following, speed adaptation has no statistical effects in steady state, whereas the presence of curves induces deviations of the USV motion from the desired path. Indeed, the USV diverges slightly from the path while turning basically because of the delay in copying the reference angular speed. Indeed, although reducing the surge speed while approaching a curve mainly according to the speed adaptation rule (11) with a preview horizon of 15 m, the vehicle does not anticipate the turning action, thus not counteracting the effects induced by yaw rate dynamics. In any event, the performance improvement due to predictive speed reduction is very significant (a factor about equal to 3 in the case of the path shown in Figure 9).

The qualitative behavior of the vehicle while following a generic path and inverting the motion direction at its ends is pointed out by a set of maneuvers

Table IV. Performance metrics: Path-following, steady-state $\bar{A}_{ss}$ (meters).

n	No speed adaptation	With speed adaptation
1	2.17	0.71
2	1.51	0.74
3	2.32	0.76

Table V. Performance metrics: steady-state $E\{\bar{A}_{ss}\}$ (meters).

	No speed adaptation	With speed adaptation
Path following, $\psi_a = 60$ deg	2.00	0.74
Line following, $\psi_a = 60$ deg	0.23	0.13
Line following, $\psi_a = 30$ deg	0.17	0.21

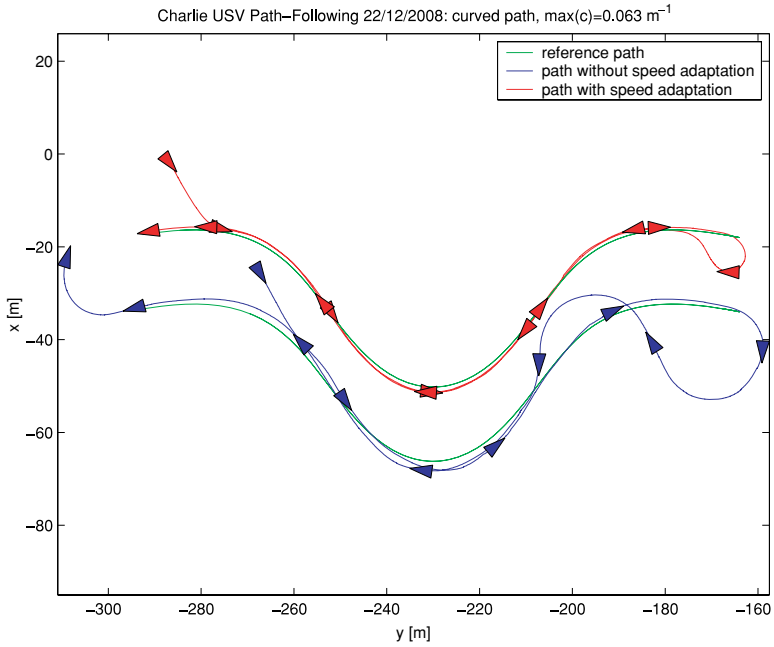

Figure 10. Path following: curved path. Charlie USV estimated and desired paths.

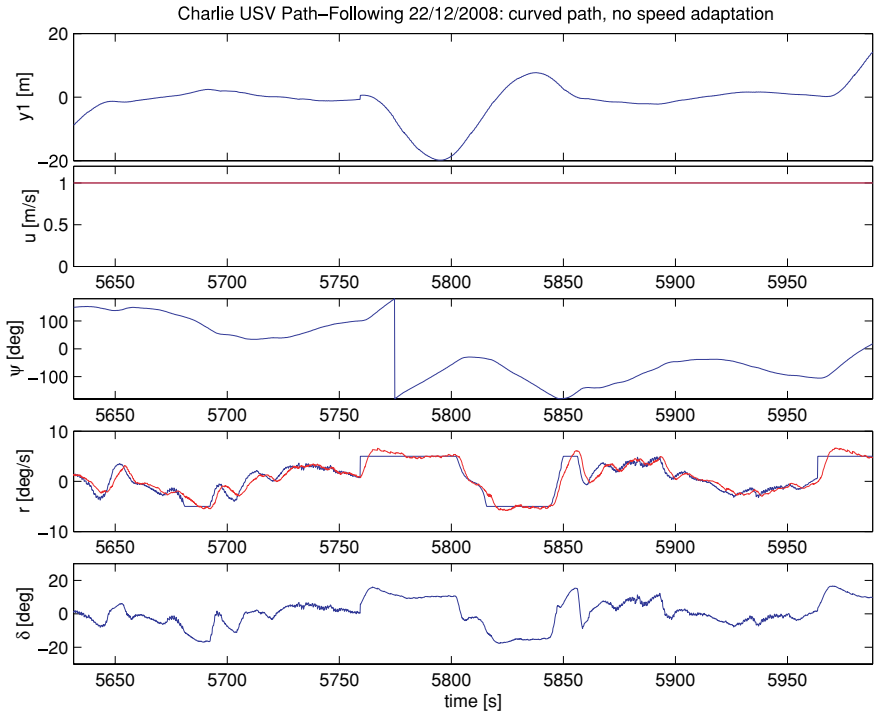

Figure 11. Path following: curved path without speed adaptation. Charlie USV path-following and navigation variables. From top to bottom: range from the desired path y_1, reference and estimated surge u^* and $\hat{u}$, estimated heading $\hat{\psi}$, reference and estimated yaw rate r^* and $\hat{r}$, and rudder angle δ.

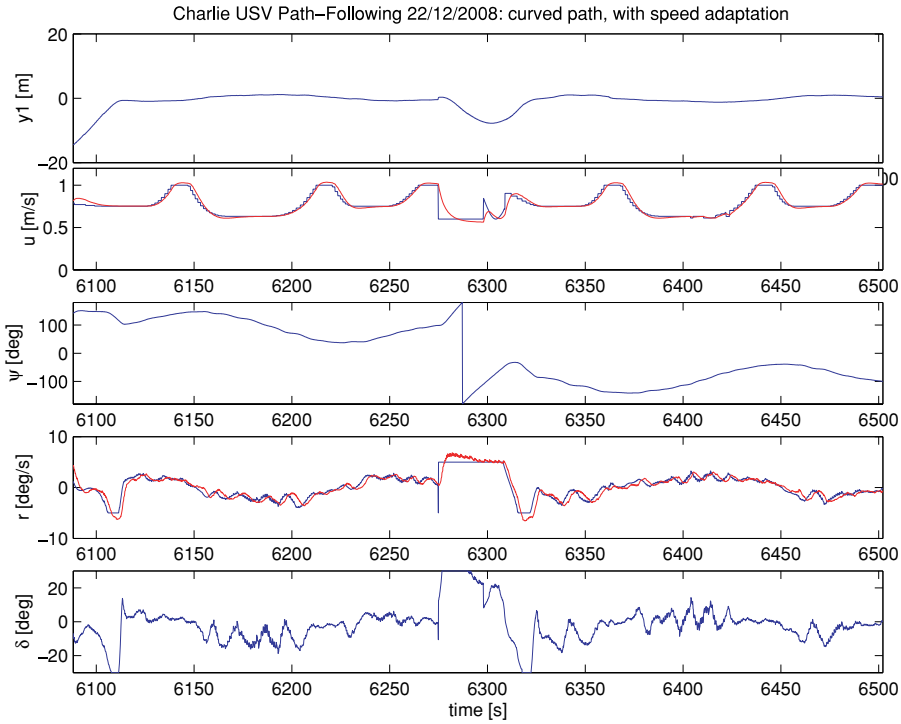

Figure 12. Path following: curved path with speed adaptation. Charlie USV path-following and navigation variables. From top to bottom: range from the desired path y_1, reference and estimated surge u^* and $\hat{u}$, estimated heading $\hat{\psi}$, reference and estimated yaw rate r^* and $\hat{r}$, and rudder angle δ.

in which the USV is requested to follow curves of shape similar to that of the previous one, but with a higher maximum curvature of 0.063 m^{-1}. The two paths were shifted in the x–y plane due to the traffic conditions inside the regatta field where the trials were performed. In this case, as is clearly visible in Figure 10, the reduction of speed while approaching a curve, given by the speed adaptation rule (11), keeps the vehicle closer to the desired path moving along high-curvature bents. Moreover, when reducing its surge while turning according to the speed adaptation rule (10), the vehicle executes U-turns in a smaller area, recovering the desired path without remarkable overshoots induced by the combination of its constrained yaw rate and high reference surge speed.

Figures 11 and 12, where the guidance and navigation variables of the USV are plotted, provide some quantitative measurements of the benefits obtained by heuristically adapting the vehicle speed. The adaptation of the surge speed down to 0.6 m/s reduces the range y_1 from the path in the Serret–Frenet frame $\langle f \rangle$ to about 1.2 m with respect to more than 2 m when no speed adaptation rule is applied. In addition, the overshoot when retracking the desired path in the opposite direction decreases from more than 7 m to about 1 m, while the approximate diameter of the U-turn decreases from about 20 m to less than 8 m. It is worth noting that the apparent higher use of the rudder when speed adaptation is applied is due to the fact that, according to the USV yaw dynamics (6), at lower surge, i.e., at lower propeller revolution rate n, higher rudder angles are required for obtaining the same yaw rate.

6. CONCLUSIONS

In this paper the problem of path following in two-dimensional space for underactuated USVs has been handled through the definition of a nonlinear Lyapunov-based guidance law, yielding convergence of the path-following error coordinates to zero.

Singularities of the algorithm are removed thanks to the introduction of the target dynamic. The proposed solution, which generates reference surge and yaw rate, has been integrated with the control system of an existing USV, managing its dynamics in a conventional nested-loop architecture. Although a rigorous demonstration of system stability is not given, the design of the path-following guidance task at the kinematic level has been validated in extended field trials carried out with the Charlie USV, developed by CNR–ISSIA and employed as a test bed for the evaluation of numerous guidance and control techniques (Caccia et al., 2007).

Moreover, experimental results confirmed the expected improvements of the tracking response of the proposed technique obtained with the integration of the guidance law with some heuristic approaches, facing the problem of speed of advance adaptation based on path curvature measurement and steering action prediction. Although these heuristic approaches introduce an algebraic loop through a coupling between the yaw and surge control inputs, dramatic benefits in terms of tracking precision and execution of human-like maneuvers have been verified experimentally.

Although experimental results show a maneuvering precision on the order of a few tens of centimeters, which is generically satisfactory for underactuated marine systems, a metric-based comparison with other guidance laws for path following proposed in the literature would allow a quantitative evaluation of system performances. The implementation and integration in the vehicle control system of a set of path-following controllers, as well as the execution of comparative trials for straight line and generic path following, is part of the Charlie USV basic research plan.

Moreover, future work focuses on the mathematical formalization of the heuristic laws and the demonstration of stability of the nested-loop guidance and control system.

ACKNOWLEDGMENTS

This work has been partially funded by the common research project "Sensor-based guidance and control of autonomous marine vehicles: Path-following and obstacle avoidance" between CNR–ISSIA Genova, Italy, and CNRS–LIRMM Montpellier, France, for the years 2006–2007, and by PRAI-FESR within the project "Coastal and harbor underwater anti-intrusion system" for the years 2005–2007. The authors wish to thank Giorgio Bruzzone and Edoardo Spirandelli for their fundamental support in developing, maintaining, and operating the Charlie USV. Special thanks to the members of A.D.P.S. Prà Sapello for their kind support to sea trials.

REFERENCES

Alves, T., Pascoal, A., Pereira, A., Rodeia, J., Simoes, A., Juliano, M., Duarte, R., Silvestre, C., Oliveira, P., Sebastiao, L., Jorge, A., & Araujo, R. (1999, March). The use of CARAVELA 2000 vehicles in operational oceanography. In Proceedings of 2nd Eurogoos Conference 1999, Rome, Italy.

Benjamin, M. R., & Curcio, J. (2004, June). COLREGS-based navigation in unmanned marine vehicles. In IEEE Proceedings of AUV-2004, Sebasco Estates, ME.

Bibuli, M., Bruzzone, G., Caccia, M., Indiveri, G., & Zizzari, A. (2008, September). Line following guidance control: Application to the Charlie unmanned surface vehicle. In Proceedings of IEEE/RSJ 2008 International Conference on Intelligent Robots and Systems, Nice, France.

Bibuli, M., Caccia, M., & Lapierre, L. (2007, September). Path-following algorithms and experiments for an autonomous surface vehicle. In Proceedings of IFAC Conference on Control Applications in Marine Systems, Bol, Croatia.

Breivik, M., & Fossen, T. I. (2004, November). Path following for marine surface vessels. In Proceedings of Oceans 2004, Kobe, Japan (pp. 2282–2289).

Breivik, M., & Fossen, T. I. (2008, December). Guidance laws for planar motion control. In Proceedings of 47th IEEE Conference on Decision and Control, Cancun, Mexico (pp. 570–577).

Bruzzone, G., Caccia, M., Bertone, A., & Ravera, G. (2008). Standard Linux for embedded real-time robotics and manufacturing control systems. Robotics and Computer Integrated Manufacturing, DOI: 10.1016/j.rcim.2007.07.016.

Caccia, M. (2006, June). Autonomous surface craft: Prototypes and basic research issues. In Proceedings of IEEE 14th Mediterranean Conference on Control and Automation, Ancona, Italy.

Caccia, M. (2007). Vision-based ROV horizontal motion control: Near-seafloor experimental results. Control Engineering Practice, 15(6), 703–714.

Caccia, M., Bibuli, M., Bono, R., & Bruzzone, G. (2008). Basic navigation, guidance and control of an unmanned surface vehicle. Autonomous Robots, 25(4), 349–365.

Caccia, M., Bibuli, M., Bono, R., Bruzzone, G., Bruzzone, G., & Spirandelli, E. (2007). Unmanned surface vehicle for coastal and protected water applications: The Charlie project. Marine Technology Socety Journal, 41(2), 62–71.

Caccia, M., Bono, R., Bruzzone, G., Bruzzone, G., Spirandelli, E., Veruggio, G., Stortini, A., & Capodaglio, G. (2005). Sampling sea surface with SESAMO. IEEE Robotics and Automation Magazine, 12(3), 95–105.

Caccia, M., Bruzzone, G., & Bono, R. (2008). A practical approach to modeling and identification of small autonomous surface craft. IEEE Journal of Oceanic Engineering. DOI: 10.1109/JOE.2008.920157.

Caccia, M., & Veruggio, G. (1999, July). Model-based heave motion estimation for variable configuration unmanned underwater vehicles. In Proceedings of IFAC World Congress, Beijing, China.

Cornfield, S. J., & Young, J. M. (2006). Unmanned surface vehicles—Game changing technology for naval operations. In Advances in unmanned marine vehicles (pp. 311–328). IEE Control Series.

Curcio, J., Leonard, J., & Patrikalakis, A. (2005, September). SCOUT—A low cost autonomous surface platform for research in cooperative autonomy. In Proceedings of Oceans 2005, Washington, DC.

Ebken, J., Bruch, M., & Lum, J. (2005, March). Applying UGV technologies to unmanned surface vessels. In SPIE Proceedings 5804, Unmanned Ground Vehicle Technology VII, Orlando, FL.

Encarnaçao, P., & Pascoal, A. (2001, December). Combined trajectory tracking and path following: An application to the coordinated control of autonomous marine craft. In Proceedings of 40th IEEE Conference on Decision and Control, Orlando, FL (vol. 1, pp. 964–969).

Fryxell, D., Oliveira, P., Pascoal, A., Silvestre, C., & Kaminer, I. (1996). Navigation, guidance and control of AUVs: An application to the MARIUS vehicle. Control Engineering Practice, 4(3), 401–409.

Gomes, P., Silvestre, C., Pascoal, A., & Cunha, R. (2006, September). A path-following controller for the DELFIMx autonomous surface craft. In Proceedings of 7th IFAC Conference on Manoeuvring and Control of Marine Craft, Lisbon, Portugal.

Indiveri, G., Zizzari, A. A., & Mazzotta, V. G. (2007, September). Linear path following guidance control for underactuated ocean vehicles. In Proceedings of 2007 IFAC Conference on Control Applications in Marine Systems, Bol, Croatia.

Lapierre, L., & Soetanto, D. (2007). Nonlinear path following control of an AUV. Journal of Oceanic Engineering, 34, 1734–1744.

Lapierre, L., Soetanto, D., & Pascoal, A. (2003, December). Adaptive, non-singular path-following of dynamic wheeled robots. In Proceedings of the 42nd IEEE Conference on Decision and Control, Maui, HI.

Majohr, J., & Buch, T. (2006). Modelling, simulation and control of an autonomous surface marine vehicle for surveying applications Measuring Dolphin MESSIN. In Advances in unmanned marine vehicles (pp. 329–352). IEE Control Series.

Manley, J. E. (2008, September). Unmanned surface vehicles, 15 years of development. In Proceedings of MTS/IEEE Oceans'08, Quebec City, Canada.

Manley, J. E., Marsh, A., Cornforth, W., & Wiseman, C. (2000, September). Evolution of the autonomous surface craft AutoCat. In Proceedings of Oceans '00, Providence, RI (vol. 1, pp. 403–408).

Martins, A., Almeida, J. M., Silva, E. P., & Pereira, F. L. (2006, September). Vision-based autonomous surface vehicle docking manoeuvre. In Proceedings of 7th IFAC Conference on Manoeuvring and Control of Marine Craft, Lisbon, Portugal.

Micaelli, A., & Samson, C. (1993). Trajectory tracking for unicycle-type and two-steering wheels mobile robots (Tech. Rep. 2097). Sophia-Antipolis, France: INRIA.

Pascoal, A., Silvestre, C., Sebastiao, L., Rufino, M., Barroso, V., Gomes, J., Ayela, G., Coince, P., Cardew, M., Ryan, A., Braithwaite, H., Cardew, N., Trepte, J., Seube, N., Champeau, J., Dhaussy, P., Sauce, V., Moitiè, R., Santos, R., Cardigos, F., Brussieux, M., & Dando, P. (2000, September). Robotic ocean vehicles for marine science applications: The European Asimov Project. In Proceedings of Oceans 2000, Providence, RI.

Pascoal, A., Silvestre, C., & Oliveira, P. (2006). Vehicle and mission control of single and multiple autonomous marine robots. In Advances in unmanned marine vehicles (pp. 353–386). IEE Control Series.

Roberts, G. (2008). Trends in marine control systems. Annual Reviews in Control, 32, 263–269.

Roberts, G., Sharif, M., Sutton, R., & Agarwal, A. (1997). Robust control methodology applied to the design of a combined steering/stabiliser system for warships. IEE Proceedings Control Theory and Applications, 144(2), 128–136.

Xu, T., Chudley, J., & Sutton, R. (2006, September). Soft computing design of a multi-sensor data fusion system for an unmanned surface vehicle navigation. In Proceedings of 7th IFAC Conference on Manoeuvring and Control of Marine Craft, Lisbon, Portugal.